Investigation of transpiration cooling in turbulent flow by DNS

By N. Christopher, J. Peter†, M. Kloker†, J.-P. Hickey

Department of Mechanical and Mechatronics Engineering, University of Waterloo, Canada

Transpiration cooling in a spatially developing turbulent boundary layer on a flat plate is simulated using direct numerical simulations (DNS). The simulations are performed by solving the compressible Navier-Stokes equations at low Mach number conditions ($M_\infty = 0.3$). Both the coolant and the hot gas are air, with isothermal walls and coolant at a temperature ratio of $T_w/T_\infty = 0.5$. In total, eight cases with transpiration cooling have been simulated, with the blowing ratios and boundary conditions being the primary parameters. By increasing the blowing ratio, it is observed that the flow changes from being dominated by wall-shear to being dominated by shear between the low-momentum coolant and high-momentum hot gas. Stevenson's log-law scaling is analysed, and reasons for its failure at high blowing rates are proposed. The heat transfer reduction to the wall is caused by the combined effects of heat advection away from the wall with blowing, and the reduction of the average boundary-layer temperature. A model for the latter effect is proposed which is physically realistic in the limit cases. Comparison to the DNS data shows good agreement in the region downstream of the transpiration zone where the heat advection term at the wall disappears. Finally, various boundary conditions are compared. It is hypothesized that for small pore sizes, neglecting the effects of the individual pores in the wall boundary condition is physically justifiable.

1. Introduction

Space transportation systems can experience very high wall temperatures and heat transfer during their operation. Combustion chamber walls are often exposed to temperatures beyond 2500 Kelvin. Similarly, re-entry vehicles experience extreme aero-thermal loads during atmospheric re-entry. These systems must rely on thermal protection systems (TPS) in order to operate safely.

One promising thermal protection system is transpiration cooling. This method of cooling has been considered recently for both the cooling of chamber walls [22], and airframe cooling on re-entry missions + [4, 9] by major aerospace organizations. For combustion chambers, transpiration cooling involves injecting some fuel as coolant through a porous material at the wall. For re-entry vehicles, either excess fuel or a dedicated coolant can be used. The perceived advantages of using transpiration cooling for re-entry vehicles is that it can reduce maintenance costs, turnaround times between launches, and enable the use of low-cost wall materials such as stainless steel.

In contrast to film cooling, the additional complexities in transpiration cooling have resulted in a lack of modelling tools and experimental data. This has inhibited the adoption of this technology for practical applications by engineers. This is despite the fact

† Institut für Aerodynamik und Gasdynamik, Universität Stuttgart, Germany

that researchers have noted that transpiration cooling is better than film cooling in terms of coolant effectiveness [1, 15] for some applications. It is therefore imperative that analytical modelling tools are developed in order for the technology to be more widely adopted. Additionally, software that couples porous-media simulations with RANS modelling requires further development, especially relating to the turbulence modelling. Recent works have started to develop this [3, 14].

Modelling the complexities of transpiration cooling is difficult since there are multiple heat transfer mechanisms involved. Inside the porous material, convection from the coolant to the solid cools the porous walls. Inside the hot gas flow, the injected coolant protects the wall from the hot gas, reducing the heat transfer into the porous material. A comprehensive simulation tool must therefore not only model the porous material, but also must be able to model the reduction of heat transfer into the porous material due to the injection of coolant. Additionally, the coolant is often injected in liquid form, and will flash to vapor inside the porous material. The phase change must be modelled in this case, since it will also affect the heat transfer.

Recently, advances in computational efficiency have allowed researchers to perform direct numerical simulation (DNS) of transpiration cooling. DNS is a valuable tool which can be used to gain unique insights into fluid flows. It is the only numerical method which fully resolves the turbulent flow in all scales; no modelling is done. Avsarkisov *et al.* [11] have performed incompressible DNS of transpiration in a spatially periodic turbulent Poiseuille flow, in order to validate a logarithmic scaling law. Kraheberger *et al.* [12] have similarly used incompressible DNS to simulate transpiration in turbulent Couette flow, and investigated the turbulent structures of the flow. In both simulations, the flow domain was periodic, with one blowing wall and one opposite suction wall in order to obtain a flow statistically independent of the streamwise location. Cerminara *et al.* [18] have performed compressible DNS of transpiration cooling in a hypersonic laminar flat-plate boundary layer, which transitions to turbulence downstream. The same group has additionally simulated coolant flow through individual spherical pores, and subsequent injection into a laminar flow [19], see also Keller & Kloker [17]; for the case of turbulent main flow and slit blowing see [16].

In this work, DNS of transpiration cooling in a subsonic turbulent flat-plate boundary layer has been simulated. The advantage of this simulation over periodic channel-flow DNS is that the flat-plate flow is truly developing spatially. Since the amount of coolant injected into the growing boundary layer will affect the amount of heat flux entering the wall, this physical phenomenon can only be captured with a spatially developing flow. By simulating this flow with DNS, details of all relevant properties of the entire 3D flow and thermal field can be obtained. This large amount of data is not feasibly obtained with present-day experimental measurements. The DNS data allows for unique insights into the physics of transpiration cooling, and can assist in validating and developing numerical models for engineering use.

2. Numerical method and computational setup

The research DNS code used in the present study is HybridX, which was developed by Johan Larsson and Ivan Bermejo-Moreno [13]. It solves the compressible Navier-Stokes (N-S) equations with a sixth-order central finite-difference for the spatial derivatives; a fourth-order Runge-Kutta scheme is used for the time integration. High-order filtering is used to stabilize the spatial scheme [10]; in the vicinity of shocks or large

density gradients, a Weighted Essentially Non-Oscillatory (WENO) scheme can be used (although it is not activated in the present work). The thermodynamic variables are related through the perfect-gas law; a 3/4 power law for viscosity is employed, as it is similar in accuracy to Sutherland's law, but with a reduced computational cost. The simulations are run in non-dimensional units for increased computational efficiency. The results can be converted to dimensional quantities for a given gas (*i.e.* air) by use of the non-dimensional parameters set in the code such as the Mach number.

A schematic of the domain can be seen in Fig. 1. The mesh is fully structured, with a wall-normal grid clustering. The number of grid points is about 118 million with $2560 \times 180 \times 256$ points respectively in the x, y, and z directions. For the baseline comparative case without injected coolant, the wall-normal resolution at $x = 30$ (*i.e.* the center of the domain) is $y_w^+ \approx 1$ with $\triangle y^+|_{\delta_{99}} \approx 6$, while the maximum streamwise and spanwise resolution is $\triangle x^+ = \triangle z^+ \approx 11$. The Mach number in the freestream is set to 0.3 in order to minimize the effect of compressibility. The Prandtl number is fixed at 0.7. Based on a unitary inlet boundary layer thickness ($\delta_i = 1$), the non-dimensional domain size is $Lx = 60$, $Ly = 6$, $Lz = 6$. For reference, this corresponds to $\delta_i \approx 5.5mm$ for the specified cases with air at a freestream temperature of 800 K.

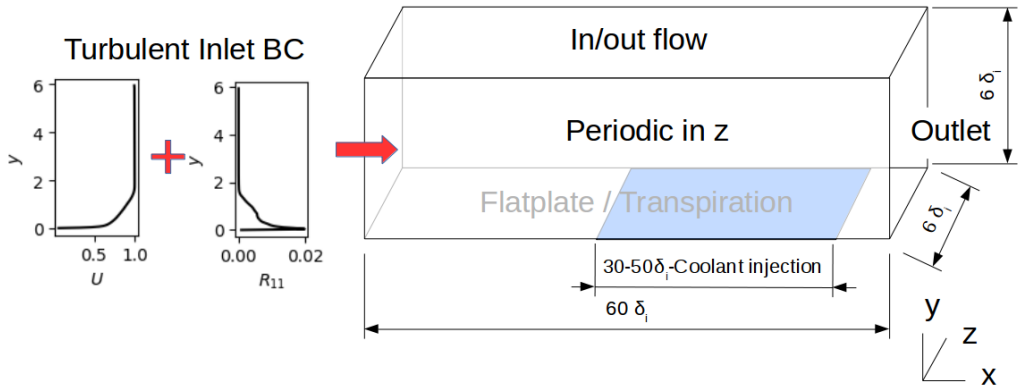

FIGURE 1. Simulation domain and illustration of inflow boundary layer turbulence.

2.1. *Boundary Conditions*

For the inlet, the average velocities and Reynolds stresses from a realistic turbulent boundary layer profile taken from [20] with $Re_\tau = 450$. Randomly generated turbulence with the desired Reynolds stress profiles is superimposed on the desired mean flow profiles at the inlet plane. Digital filtering, in both space and time, assures a more realistic correlation length of the turbulent fluctuations. At the top and outlet of the domain, in/outflow boundaries are specified which use a Summation-By-Parts (SBP) scheme with a Simultaneous Approximation Term (SAT) penalty to compute the fluxes. Sponge layers are applied to the outlet boundary in order to reduce numerical reflections. The domain is periodic in the z direction.

For the transpiration-wall modelling, no-slip conditions have been applied in the x and z directions. In the y direction, the wall-normal velocity is set depending on the case. The fluid is the same for both the hot gas and coolant. It has been assumed that the coolant is injected in a laminar state. This is often the case, due to very small pore channels resulting in low pore Reynolds numbers. Two different treatments for the

velocity profile of the injected coolant have been used in this study. The first is a constant velocity over the transpiration region, which will be denoted as uniform blowing. The second is a parabolic profile which would be observed in a laminar channel flow, with the wall-normal velocity varying in the streamwise direction only. This profile is then repeated multiple times over the transpiration region. These spanwise-aligned slits are separated by regions of impermeable, no-slip walls. This second profile is denoted as slit blowing, since it models blowing of coolant from multiple sits. A visual representation of the transpiration wall boundary conditions (BC) is shown in Fig. 2.

At the blowing boundary, the temperature is prescribed, the pressure is taken from the flow domain, and the density is computed to satisfy the ideal gas law. These thermodynamic conditions are used to compute the fluxes at the boundary. It should be noted that because of this condition, there is a slight difference in the density and therefore mass flux of coolant injected from the leading to trailing edge of the transpiration region. This is due to the slight pressure gradient on the plate that is induced by the injection of coolant. However, this difference is small, and therefore is not considered significant (it is on the order of 1% for the highest blowing ratio).

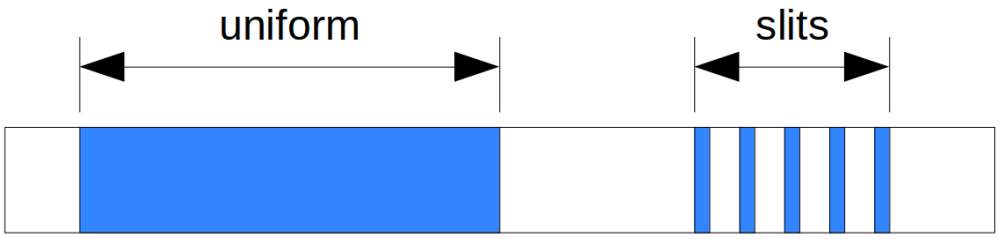

FIGURE 2. Transpiration BCs. Blue represents regions where $v \neq 0$, white an impermeable wall.

The reason for simulating both uniform injection and slit blowing is to gain insight into the effects of the different boundary conditions on the flow properties. Since modelling individual pores is generally non-feasible in practical CFD applications, the assumption of a uniform blowing area is often made. By leaving regions of solid wall between the slits, some insight into the effect of individual pores and the validity of the uniform injection BC can be gained.

2.2. *Simulated Cases*

In total, 10 cases have been simulated: 4 uniform blowing cases, 4 slit blowing cases, and 2 reference cases with no blowing. For the reference simulations, both an adiabatic and an isothermal case were simulated in order to validate the domain against other results found in literature. The adiabatic case will not be discussed in detail, however it should be noted that the results are in good agreement with the data from [20]. For the isothermal simulation, at the center of the domain (x=30), the Reynolds numbers are: $Re_\tau = 600$, $Re^*_\tau = 260$, $Re_\theta = 790$, $Re_{\delta 2} = 1320$. At the same location, the non-dimensional wall heat transfer rate is $B_q = q_w/(\rho_w c_p u_\tau T_w) = 0.043$.

The differences between the cases are highlighted in Tab. 1. For all cases in Tab. 1, an isothermal wall boundary condition of $T_w/T_\infty = 0.5$ is used, and the coolant is injected at $T_c = T_w$. The subscripts ∞, c, and w correspond to the freestream, coolant gas at injection, and wall quantities respectively. It should be noted that the blowing ratio is defined as $F = \rho_c \mathbf{V}_c/\rho_\infty U_\infty$, where $\mathbf{V}$ is the average Darcy velocity. In mathematical

Simulations	**Blowing ratio**, F	**Notes**
Flatplate2	0	
Uniform-2%-1	0.02	
Uniform-2%-2	0.02	injection from $x_a = 30$ to $x_b = 40$
Uniform-0.6%	0.006	
Uniform-0.2%	0.002	
Slits-2%-1	0.02	slit width is 0.234 in x
Slits-2%-2	0.02	slit width is 0.469 in x
Slits-0.6%-1	0.006	slit width is 0.234 in x
Slits-0.6%-2	0.006	slit width is 0.469 in x

TABLE 1. Parameters of the simulated cases.

terms

$$\mathbf{V} = \frac{1}{x_b - x_a} \int_{x_a}^{x_b} V dx,$$

where x_a and x_b are the beginning and end of the transpiration region ($x_a = 30$ and $x_b = 49.6$ for all cases except the Uniform-2%-2 case). For all the slit simulations, the ratio of blowing area to total wall area (*i.e.* the wall porosity) is $1/3$.

3. Results

3.1. *Validation*

In order to validate the simulation setup, the isothermal wall reference simulation is compared to results in literature. In order to compare the data, a proper scaling needs to be applied. Since the flows simulated here incorporate both compressibility and heat transfer, the transformations proposed by Trettel and Larsson [2] are used. Since no other DNS data for low Mach number compressible flows with heat transfer was found, the cases are compared to incompressible adiabatic turbulent flat-plate data from [20]. The comparison can be seen in Fig. 3.

Figure 3(a) shows that with the proper scaling applied to the data, the results collapse in the inner layer. It should be noted that when the Van Driest transformation is applied, the scaling does not match the adiabatic incompressible data.

Figure 3(b) compares the turbulent intensities in the inner layer to reference incompressible adiabatic data. It should be mentioned again that the present data uses the scalings suggested by Trettel and Larsson [2], which for Fig. 3(b) would be Morkovin's scaling, with semilocal scaling for y^+. While the results generally agree, there is a higher peak in the streamwise turbulence intensity for the present data. It has been shown by other works that this peak does increase for supersonic and hypersonic compressible flows with heat transfer [8, 23]. As previously mentioned, no other DNS of a subsonic compressible turbulent flat-plate flow with heat transfer was found in the review of literature. Based on the present data, the increase in peak streamwise turbulence intensity still exists in the subsonic regime.

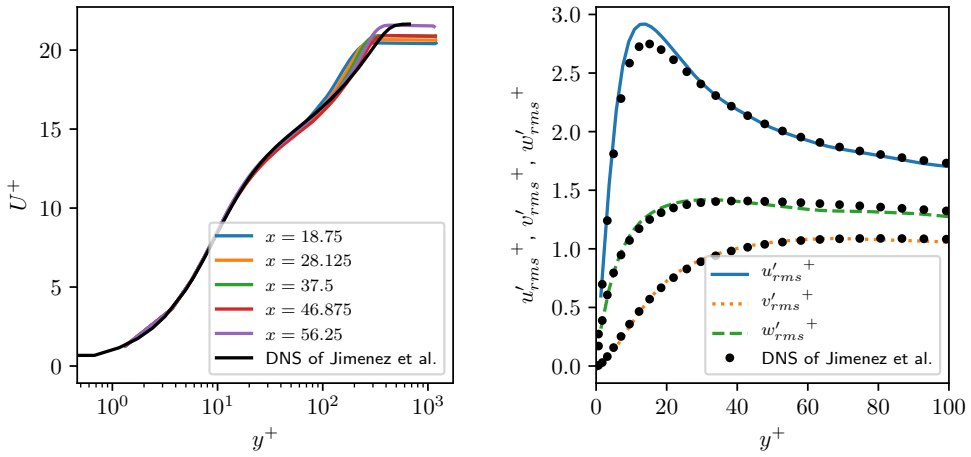

(a) Law of the wall scaling. (b) Turbulent intensities at x = 46.875.

FIGURE 3. Cooled flatplate simulation (Flatplate2) scaled following Trettel and Larsson [2], compared to incompressible adiabatic flatplate DNS from [20] at $Re_\theta = 1100$.

3.2. *Effect of blowing ratio on turbulence*

In this section, we compare the results at the three different blowing ratios with uniform injection (*i.e.* Uniform-2%-1, Uniform-0.6%, and Uniform-0.2%). The purpose of comparing these three cases is to investigate the effect that the blowing rate has on the flow turbulence. This is important, since the turbulence can have significant effects on both the heat transfer and drag.

The turbulent kinetic energy (TKE) can be used to quantify the effect of the blowing ratio on the production of turbulence. The TKE for the three blowing rates is shown in Fig. 4. It can be seen that for the lowest blowing ratio, the TKE remains relatively unchanged in structure and magnitude within the region where coolant is injected. However, for the high blowing ratio the TKE is greatly enhanced away from the wall. The reasoning for this effect appears to be that the large amount of coolant injected causes the incoming boundary layer to separate from the wall. This causes the formation of a low-momentum cold gas layer near the wall which causes a shear layer to form with the high-momentum hot gas above.

To supplement the TKE plots, the diagonal terms of the Reynolds stress tensor are shown in Fig. 5 at x= 40 (in the transpiration region) and at x=55 (after the transpiration region). In order to compare the data in a meaningful way, no (inner) scaling has been applied for these plots. This is because the wall shear stress decreases with increasing blowing rate, so applying a scaling would show that a higher blowing ratio has a lower normalized stress (which is not physically insightful). Inside the transpiration zone, the highest blowing ratio no longer shows a peak in R_{11} near the wall. Instead, the TKE maximum is pushed away from the wall. This is in agreement with a separated flow. Downstream of the transpiration, a peak in R_{11} close to the wall begins to grow again. In the lower blowing ratio cases, the R_{11} stress is increased in the outer region of the boundary layer, however the peak close to the wall does not increase - it actually decreases downstream. The R_{22} and R_{33} stresses increase for all cases in comparison to the reference case.

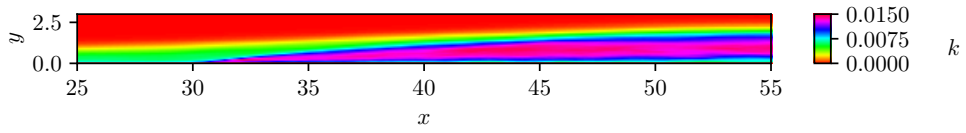

(a) Uniform-2%-1 ($F = 2\%$).

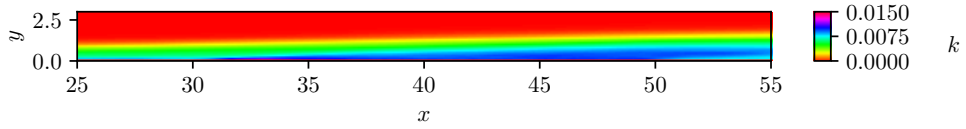

(b) Uniform-0.6% ($F = 0.6\%$).

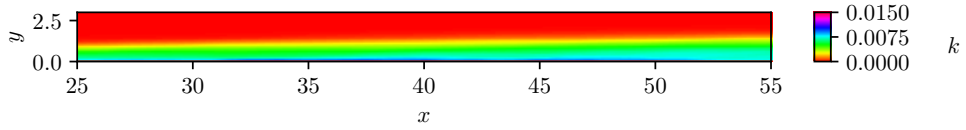

(c) Uniform-0.2% ($F = 0.2\%$).

FIGURE 4. Temporal and spanwise average turbulent kinetic energy at different blowing rates.

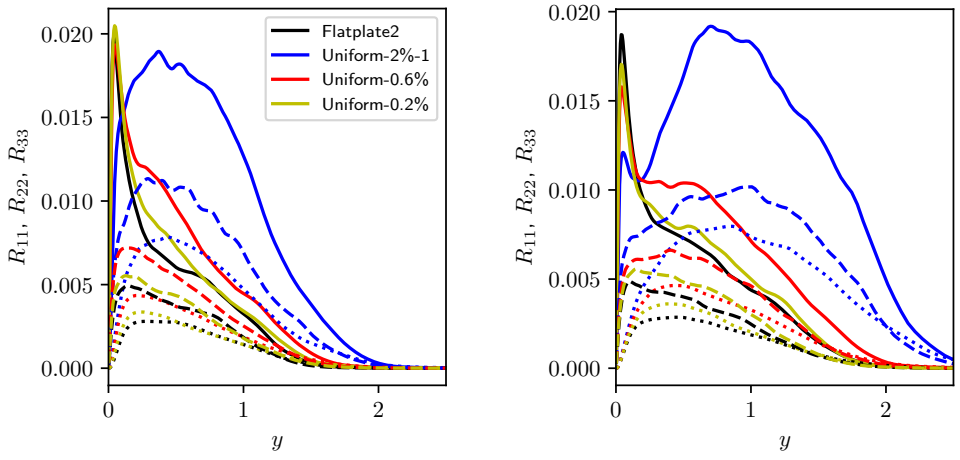

(a) Stresses at x=40.

(b) Stresses at x=55.

FIGURE 5. Trace of averaged Reynolds stress tensor vs y. R_{11} ——— ; R_{22} ····· ; R_{33} – – – – .

3.3. *Cooling effectiveness*

In the DNS, the ratio of the heat fluxes between the reference case and the cases with transpiration cooling can be used to compute the cooling effectiveness:

$$\eta = 1 - \left.\frac{q_{transpiration}}{q_{flatplate}}\right|_w \tag{3.1}$$

3.3.1. η *Model*

One very successful model in predicting η for film cooling looks at the energy balance in the boundary layer [21]. For gas-in-gas cooling, assuming that $\overline{T} \approx T_{w,ad}$ (where $\overline{T}$ is the average boundary layer temperature, and $T_{w,ad}$ is the adiabatic wall temperature), the cooling effectiveness can be modelled as:

$$\eta = \frac{1}{1 + \frac{\dot{m}_\infty C_{p,\infty}}{\dot{m}_c C_{p,c}}} \tag{3.2}$$

The main unknown in this model is the ratio of $\dot{m}_\infty/\dot{m}_c$. $\dot{m}_\infty$ is typically assumed to develop according to the $\frac{4}{5}$th law for turbulent boundary layer growth:

$$\dot{m}_\infty = 0.329 \rho_\infty U_\infty x' Re_{x'}^{-1/5} \tag{3.3}$$

For the coolant, it is assumed that $\dot{m}_c = \rho_c V_c x"$. For film cooling, $x" = s$ is the slot width. Since the slot width is a constant, film cooling models are only valid starting at the trailing edge of the slot.

For film cooling, there are multiple models that employ the above assumptions, which vary based on their definition of where x' starts. These models generally assume that at the slot, the effectiveness is unity. Other forms of η that do not follow Equation 3.2 can approach a value of infinity at the slot, and are only meant to be used at some distance downstream once η drops below one [21]. Neither of these bode well for transpiration cooling, since there must be a finite amount of heat entering the solid inside the transpiration region. However, this generally arises due to the fact that $\dot{m}_c$ is assumed to be a constant, independent from streamwise position.

The classical film cooling effectiveness models must be modified for use inside the transpiration region. Specifically, the amount of coolant injected must be a function of the location in x. On this basis, we choose $\dot{m}_c = \int_0^x \rho_c V_c dx$, and $x = 0$ at the leading edge of the porous plate. It is also assumed that this is the location where the turbulent boundary layer starts (*i.e.* $x' = x$). Using these assumptions, we arrive at the following relationship:

$$\frac{\dot{m}_\infty}{\dot{m}_c} = 0.329 \left(\frac{\rho_\infty U_\infty x}{\int_0^x \rho_c V_c dx}\right)^{0.8} \left(\frac{\int_0^x \rho_c V_c dx}{\mu_\infty}\right)^{-0.2} \tag{3.4}$$

The resulting cooling effectiveness has the desired form in the limit cases. At $x \to 0^+$, $\eta \to 0$. Since no coolant has been injected yet, this is the logical value. For a finite transpiration region, as $x \to \infty$, $\eta \to 0$. For an infinitely long transpiration region, as $x \to \infty$, $\eta \to 1$.

Comparing the model for η using Eq. (3.4) to the present DNS data in Fig. 6, it is evident that this model works reasonably well downstream of the transpiration zone. Due to the success of film cooling theory over the past 50 years, this is not surprising. After the transpiration zone, the effects of transpiration cooling on the heat transfer are

essentially the same as film cooling. Evidently, other cooling effectiveness models have been proposed for post-transpiration regions based on experimental data [5], however as mentioned previously they are not consistent in the transpiration region.

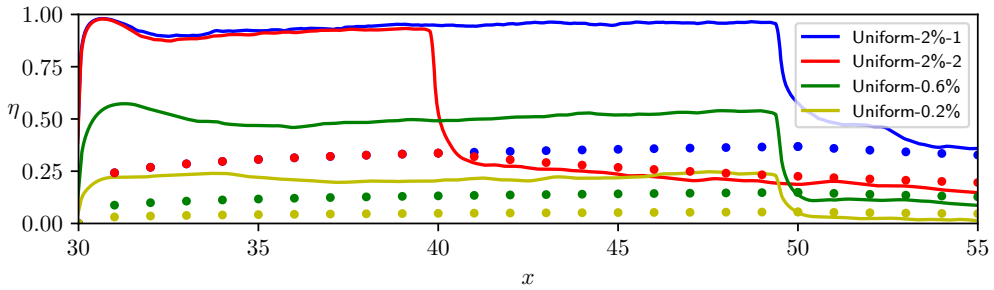

FIGURE 6. Film accumulation effectiveness. present data ——— ; model • .

In Fig. 6 it can be seen that inside the transpiration region, this model is not sufficient in order to account for the reduction in heat flux. This can be explained by the modification of terms in the energy equation due to the non-zero value of V near the wall; there is advection of heat away from the wall due to the blowing velocity. This effect is not described by the model.

3.4. *Log-law scaling*

The injected coolant shifts the law of the wall. This shift has been studied for over half a century in the context of suction and blowing walls, and many relationships have been proposed in an attempt to generalize the problem. A summary of many of these relationships can be found in [6]. The fact that there are so many different proposed relationships speaks to the lack of a universally applicable transformation.

One way of deriving a log-law relationship is to incorporate the effect of the blowing wall on the shear stress. The assumption is that the x-momentum equation simplifies to $\rho v_w dU/dy = d\tau/dy$. One such relationship using the above assumptions is proposed by Stevenson [7]:

$$\frac{2}{V_w^+}(\sqrt{V_w^+ U^+ + 1} - 1) = \frac{1}{\kappa} ln(y^+) + B \tag{3.5}$$

where $V_w^+ = V_w/u_\tau$. This relationship is compared to the present data in Fig. 7, with $B = 5.1$ and $\kappa = 0.41$. For the low blowing ratio the transformation is accurate, however it is clear that this relationship fails at higher blowing ratios.

One of the possible reasons for the failure of the scaling is due to the underlying assumptions that are discussed below. After applying the Reynolds decomposition to the N-S momentum equation and neglecting higher-order terms, the equation becomes:

$$(\overline{\rho}\,\overline{u_j} + \overline{\rho' u_j'})\frac{\partial \overline{u_i}}{\partial x_j} \approx -\frac{\partial \overline{p}}{\partial x_i} + \frac{\partial}{\partial x_j}(\overline{\sigma_{ij}} - \overline{\rho} \overline{u_i' u_j'}) \tag{3.6}$$

In the derivation for the blowing/suction scaling laws, the incompressible form is used (*i.e.* $\overline{\rho' u_j'} = 0$), the pressure term is neglected, the gradients in x and z are assumed negligible, and it is assumed that $\overline{u_2} = V_w$. These assumptions simplify the equation to $\rho V_w dU/dy = d\tau/dy$. This is then used in conjunction with the assumption of $\tau/\rho = (\kappa y \frac{\partial U}{\partial y})^2$ in order to derive the scaling [7].

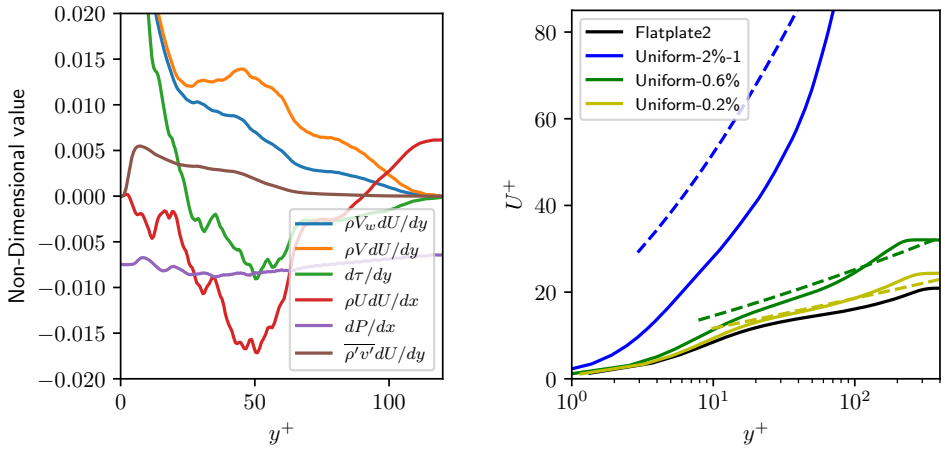

(a) x-momentum Navier-Stokes terms. Uniform-2%-2 simulation at $x = 37$. (b) law of the wall at $x = 47$. Scaled data ——— ; Stevenson law – – – – .

FIGURE 7. Analysis of Stevenson's log-law model.

To check these assumptions, the most significant terms in the compressible N-S x-momentum equation have been plotted in Fig. 7(a). It is evident that the simplification of the N-S equation is not valid. First, the assumption that $V = V_w$ leads to error in the log layer. Additionally, there is a compressible term $\overline{\rho' v'}$ which is present and non-negligible. Also, due to the nature of the transpiration, there is a nonzero pressure gradient, which results in non-negligible streamwise gradient (*i.e.* $d/dx \neq 0$)

3.5. *Slits vs Uniform Blowing*

In order to gain insight on the effect of individual pores, we compare the slit simulations with the uniform blowing simulations. This is done to primarily assess the validity of the uniform blowing boundary condition, since simulations with pore-resolved boundary conditions are currently not feasible for practical applications. It should be noted that the slit width simulated is large in relation to the pore sizes which would be used in a real transpiration cooling case. This is simply due to computational cost. Two different slit widths were simulated in order to identify trends in the results as the pore size approaches the realistic case for transpiration cooling.

First, we consider the effect of the slits on the flow turbulence. Figure 8 compares the turbulent kinetic energy for the $F = 2\%$ cases with different slits (Fig. 4(a) shows the corresponding uniform blowing case). The most notable difference between the uniform and slit BCs is that in the slit cases there is an area of low TKE in the near-jet region. The reason for this low TKE region is that the individual slits have a higher momentum than the corresponding region in the uniform BC. This means that the higher momentum coolant is able to penetrate deeper into the flow without being disturbed. It should be noted that this is in part a consequence of the fixed velocity laminar BC applied for the blowing slits. In a real film cooling flow, the freestream turbulence may impinge into the coolant channel [16]. For the case with smaller slits, the jets do not penetrate as deep into the domain before being broken up. This suggests that as the slit size gets smaller, the effects of the individual jets is reduced. In the rest of the flow domain, the turbulence is minimally disturbed by the difference in boundary condition. Based on

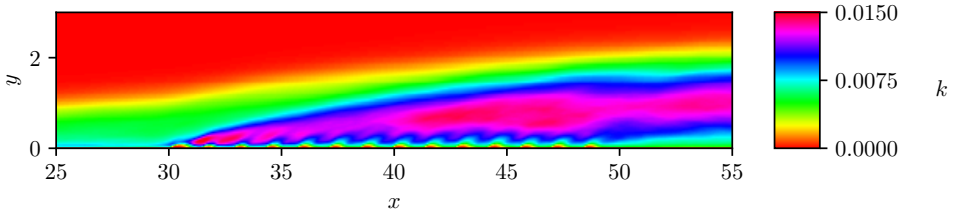

(a) Slits-2%-2.

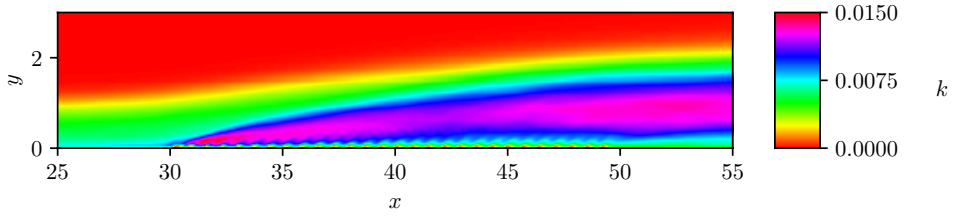

(b) Slits-2%-1.

FIGURE 8. Turbulent kinetic energy comparison for different BCs.

these observations, it is feasible that for small pore sizes, a uniform blowing BC can realistically predict the flow turbulence.

It is also imperative to consider the effect of the slits on the heat flux entering the wall. Figure 9 compares the cooling effectiveness for cases with $F = 0.6\%$. The slit cases have a periodic cooling effectiveness, which corresponds to the individual slits of injected coolant. At the region of the slit, the wall-normal velocity is high, resulting in high heat advection and also a high cooling effectiveness. However, between the slits, the wall-normal velocity at the wall returns to zero. This means that the heat advection term disappears at the wall between the slits.

It is also apparent that if there is a low amount of turbulence near the wall due to the slits, this could also cause the periodic effect. For this reason, we look at the turbulent transport of heat to the wall via $\overline{v'T'}$. This is shown in Fig. 10. It appears that the difference in turbulent transport of heat due to the BC is relatively small.

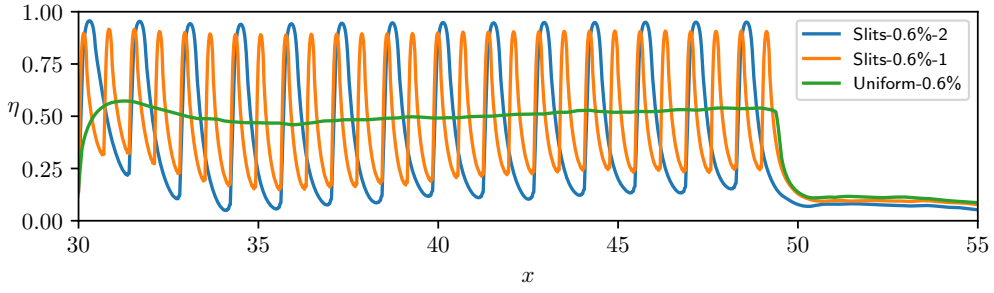

FIGURE 9. Film accumulation effectiveness. $F = 0.6\%$.

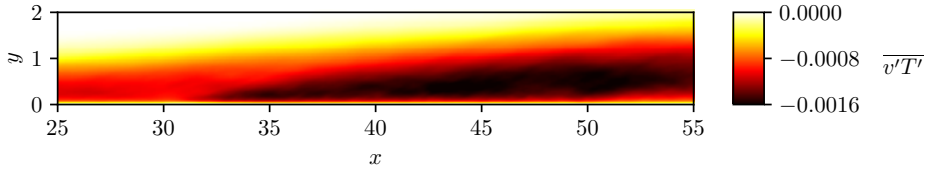

(a) Uniform-0.6%.

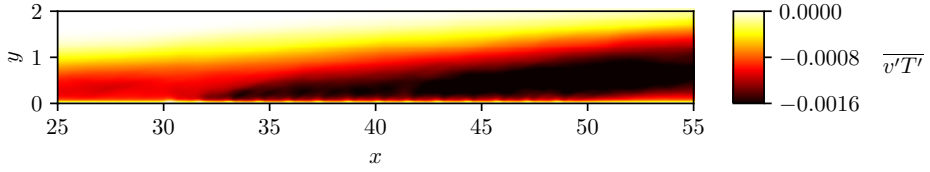

(b) Slits-0.6%-2.

FIGURE 10. Turbulent transport of heat.

4. Conclusions

Direct Numerical Simulations of transpiration cooling in a spatially-developing turbulent flat-plate boundary layer have been performed. These simulations serve to gain insight into the physics of transpiration cooling, and to analyze and propose modelling strategies for heat flux and velocity boundary conditions.

At low blowing ratios (*i.e.* $F = 0.2\%$), there is a small increase in the TKE in comparison to the reference isothermal flat-plate case, but the form of the turbulent stresses remains relatively unchanged. At higher blowing ratios (*i.e.* $F = 2\%$) the hot gas flow separates from the wall, and the peak in TKE is caused by the interaction between high-momentum hot gas and low-momentum coolant gas (rather than the shear at the wall). Downstream of the transpiration zone, the shear at the wall re-grows.

There are effectively two mechanisms which contribute to the reduction of wall heat transfer in the transpiration zone. The first is the reduction in average temperature of the boundary layer due to the injected coolant. An equation for predicting this effect has been proposed, and is consistent in the limit cases. By comparing the data downstream of the transpiration zone, it can be seen that the proposed model is successful in predicting this phenomenon. The second heat reduction mechanism is heat advection away from the wall. In the transpiration zone, this appears to be the dominating heat-transfer reduction mechanism. Future work will involve combining models of this effect with the model proposed in this paper, and comparing to the DNS data.

Many log-law scalings have been proposed over the years for blowing walls. One classical scaling proposed by Stevenson [7] has been compared to the present DNS data, and shown to only work for low blowing ratios. By analyzing the terms in the x-momentum equation, it is shown that the underlying assumptions of Stevenson's scaling (and other scalings that use similar derivations) do not hold for high blowing ratios.

Comparing the cases simulated with uniform injection to the cases with blowing by discrete slits, some differences are apparent. The TKE is reduced near the slits due to the relatively high wall-normal momentum of the coolant. Additionally, the increased heat advection away from the wall at the slits reduces the heat transfer in that region, but the heat transfer between the slits is increased. However, these effects are mitigated by decreasing the slit width (at constant integral coolant mass flux). It is hypothesized that for small pore sizes, the use of uniform blowing BCs is realistic.

Acknowledgments

Financial support has been provided by the German Research Foundation (Deutsche Forschungsgemeinschaft – DFG) in the framework of the Sonderforschungsbereich Transregio 40, SFB-TRR40.

References

[1] ECKERT, E.R.G. AND LIVINGOOD, J.N. (1953). *Comparison of effectiveness of convection-, transpiration-, and film-cooling methods with air as coolant*. Tech. Rep. Report 1182, National Advisory Committee for Aeronautics.

[2] TRETTEL, A. AND LARSSON, J. (2016). Mean velocity scaling for compressible wall turbulence with heat transfer. *Physics of Fluids*, **28**(2). ISSN 10897666. DOI 10.1063/1.4942022.

[3] DAHMEN, W., MÜLLER, S., ROM, M., SCHWEIKERT, S., SELZER, M. AND VON WOLFERSDORF, J. (2015). Numerical boundary layer investigations of transpiration-cooled turbulent channel flow. *International Journal of Heat and Mass Transfer*, **86**, 90–100. ISSN 00179310. DOI 10.1016/j.ijheatmasstransfer.2015.02.075. URL http://dx.doi.org/10.1016/j.ijheatmasstransfer.2015.02.075.

[4] D'AGOSTINO, R. (2019). Elon Musk: Why I'm Building the Starship out of Stainless Steel. URL https://www.popularmechanics.com/space/rockets/a25953663/elon-musk-spacex-bfr-stainless-steel/.

[5] GOLDSTEIN, R.J., SHAVIT, G. AND CHEN, T.S. (1965). Film-Cooling Effectiveness With Injection Through a Porous Section. *Journal of Heat Transfer*, **87**(3), 353. ISSN 00221481. DOI 10.1115/1.3689114.

[6] FERRO, M. (2017). *Experimental study on turbulent boundary-layer flows with wall transpiration*. Ph.D. thesis, KTH Royal Institute of Technology.

[7] STEVENSON, T. (1963). *A law of the wall for turbulent boundary layers with suction or injection*. Tech. Rep. 166, Cranfield College of Aero.

[8] SHAHAB, M.F., LEHNASCH, G., GATSKI, T.B. AND COMTE, P. (2011). Statistical characteristics of an isothermal, supersonic developing boundary layer flow from DNS data. *Flow, Turbulence and Combustion*, **86**(3-4), 369–397. ISSN 13866184. DOI 10.1007/s10494-011-9329-0.

[9] VAN FOREEST, A., SIPPEL, M., KLEVANSKI, J., GÜLHAN, A. AND ESSER, B. (2007). Transpiration cooling to handle the aerothermodynamic challenges of the spaceliner concept. In: *2nd European Conference for Aerospace Sciences (EUCASS)*.

[10] MATTSSON, K., SVÄRD, M. AND NORDSTRÖM, J. (2004). Stable and accurate artificial dissipation. *J. Sci. Comput.*, **21**, 57–79. DOI 10.1023/B:JOMP.0000027955.75872.3f.

[11] AVSARKISOV, V., OBERLACK, M. AND HOYAS, S. (2014). New scaling laws for turbulent Poiseuille flow with wall transpiration. *Journal of Fluid Mechanics*, **746**, 99–122. ISSN 14697645. DOI 10.1017/jfm.2014.98.

[12] KRAHEBERGER, S., HOYAS, S. AND OBERLACK, M. (2017). DNS of a turbulent Couette flow at constant wall transpiration up to Re_τ=1000. *Journal of Fluid Mechanics*, 421–443. ISSN 14697645. DOI 10.1017/jfm.2017.757.

[13] BERMEJO-MORENO, I., BODART, J., LARSSON, J., BARNEY, B.M., NICHOLS, J.W. AND JONES, S. (2013). Solving the compressible navier-stokes equations on up to 1.97 million cores and 4.1 trillion grid points. In: *SC '13: Proceedings of the*

International Conference on High Performance Computing, Networking, Storage and Analysis. ISSN 2167-4337. DOI 10.1145/2503210.2503265.

[14] DING, R., WANG, J., HE, F., DONG, G. AND TANG, L. (2019). Numerical investigation on the performances of porous matrix with transpiration and film cooling. *Applied Thermal Engineering*, **146**(September 2018), 422–431. ISSN 13594311. DOI 10.1016/j.applthermaleng.2018.09.134. URL https://doi.org/10.1016/j.applthermaleng.2018.09.134.

[15] MIN, Z., HUANG, G., PARBAT, S.N., YANG, L. AND CHYU, M.K. (2019). Experimental investigation on additively manufactured transpiration and film cooling structures. *Journal of Turbomachinery*, **141**(3), 1–10. ISSN 15288900. DOI 10.1115/1.4042009.

[16] KELLER, M.A. AND KLOKER, M.J. (2016). Direct Numerical Simulation of Foreign-Gas Film Cooling in Supersonic Boundary-Layer Flow. *AIAA Journal*, **55**(1), 99–111. ISSN 0001-1452. DOI 10.2514/1.j055115.

[17] KELLER, M.A. AND KLOKER, M.J. (2014). Effusion Cooling and Flow Tripping in Laminar Supersonic Boundary-Layer Flow. *AIAA Journal*, **53**(4), 902–919. ISSN 0001-1452. DOI 10.2514/1.j053251.

[18] CERMINARA, A., DEITERDING, R. AND SANDHAM, N. (2019). Parallel multiscale simulation of hypersonic flow with porous wall injection. In: Ivanyi, P. and Topping, B. (Eds.), *Proceedings of the Sixth International Conference on Parallel, Distributed, GPU and Cloud Computing for Engineering*, vol. 112. Civil-Comp Press, United Kingdom. ISBN 978-1-905088-67-6.

[19] CERMINARA, A., DEITERDING, R. AND SANDHAM, N. (2018). Direct numerical simulation of hypersonic flow through regular and irregular porous surfaces. In: *Proceedings of the Seventh European Conference on Computational Fluid Dynamics, ECCOMAS ECFD 2018*.

[20] JIMÉNEZ, J., HOYAS, S., SIMENS, M.P. AND MIZUNO, Y. (2010). Turbulent boundary layers and channels at moderate Reynolds numbers. *Journal of Fluid Mechanics*, **657**, 335–360. ISSN 00221120. DOI 10.1017/S0022112010001370.

[21] GOLDSTEIN, R.J. (1971). Film Cooling. In: Irvine, T.F. and Hartnett, J.P. (Eds.), *Advances in Heat Transfer*, vol. 7. Elsevier, 321–379. DOI https://doi.org/10.1016/S0065-2717(08)70020-0. URL http://www.sciencedirect.com/science/article/pii/S0065271708700200.

[22] HERBERTZ, A., ORTELT, M., MÜLLER, I. AND HALD, H. (2014). c*-Efficiency evaluation of transpiration cooled ceramic combustion chambers. *CEAS Space Journal*, **6**(2), 99–105. ISSN 18682510. DOI 10.1007/s12567-014-0062-0.

[23] ZHANG, C., DUAN, L. AND CHOUDHARI, M.M. (2018). Direct Numerical Simulation Database for Supersonic and Hypersonic Turbulent Boundary Layers. *AIAA Journal*, **56**(11), 1–15. ISSN 0001-1452. DOI 10.2514/1.J057296. URL https://arc.aiaa.org/doi/10.2514/1.J057296.